Communication

# Time-Resolved Ultraviolet Photodissociation Mass Spectrometry Probes the Mutation-Induced Alterations in Protein Stability and Unfolding Dynamics

Pan Luo,[#] Zheyi Liu,[#] Can Lai, Zhixiong Jin, Mengdie Wang, Heng Zhao, Yu Liu, Weiqing Zhang, Xingan Wang, Chunlei Xiao, Xueming Yang, and Fangjun Wang*

Read Online

ACCESS | 📊 Metrics & More | 📰 Article Recommendations | 🆘 Supporting Information

**ABSTRACT:** How mutations impact protein stability and structure dynamics is crucial for understanding the pathological process and rational drug design. Herein, we establish a time-resolved native mass spectrometry (TR-nMS) platform via a rapid-mixing capillary apparatus for monitoring the acid-initiated protein unfolding process. The molecular details in protein structure unfolding are further profiled by a 193 nm ultraviolet photodissociation (UVPD) analysis of the structure-informative photofragments. Compared with the wild-type dihydrofolate reductase (WT-DHFR), the M42T/H114R mutant (MT-DHFR) exhibits a significant stability decrease in TR-nMS characterization. UVPD comparisons of the unfolding intermediates and original DHFR forms indicate the special stabilization effect of cofactor NADPH on DHFR structure, and the M42T/H114R mutations lead to a significant decrease in NADPH-DHFR interactions, thus promoting the structure unfolding. Our study paves the way for probing the mutation-induced subtle changes in the stability and structure dynamics of drug targets.

Proteins undergo dynamic structure changes over a broad range of time scales, which can be mainly divided into
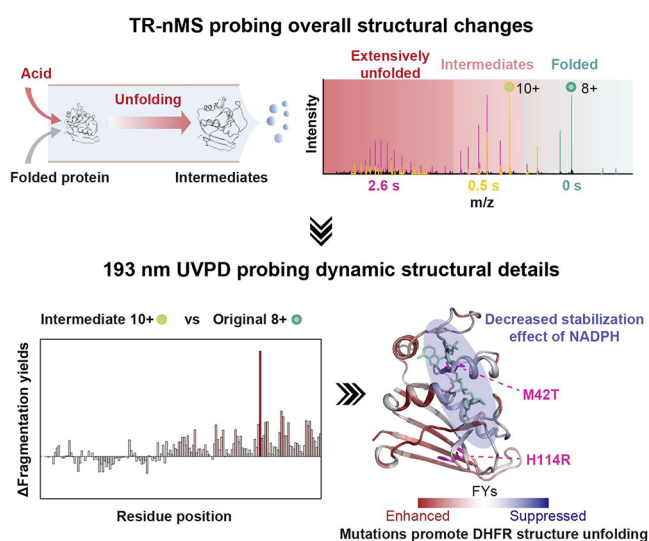


**Figure 1.** Schematic diagram of TR-nMS and 193 nm UVPD for the exploration of mutation-induced alterations on protein stability and unfolding dynamics.

slight thermally driven structure fluctuations at equilibrium and large-scale structure rearrangements under nonequilibrium transitions.[1,2] Considering the dynamic properties of proteins in performing biological functions, it is of great significance to analyze their stability and structure dynamics in both physiological and pathological processes. Pathogenic mutations with dysregulation on protein stability, structure dynamics, and activity widely exist in disease processes such as cancer and neurodegenerative diseases.[3−5] Furthermore, protein pathogenic mutation is one of the most common reasons for drug resistance.[6,7] How mutation affects protein structure is essential for understanding the molecular mechanism of disease, as well as targeted drug design. However, it is still a great challenge to probe the molecular details of mutation-induced subtle structure dynamics and usually computational methods are utilized for the prediction of mutation related alterations.[8,9]

Recently, native mass spectrometry (nMS) with non-denaturing electrospray ionization (nESI) has become a powerful tool for monitoring the protein dynamic structures and protein−protein interactions with the advantages of high sensitivity, high throughput, and can simultaneously detect different components in complex mixtures.[10−14] To get the molecular details of protein structure changes, the native top-down MS (nTDMS) strategy can be utilized with the combination of advanced dissociation methods such as ultraviolet photodissociation (UVPD)[15,16] and electron capture/transfer dissociation (ExD).[17−19] It is demonstrated that 193 nm UVPD can provide rich types of structure-informative photofragments for the characterization of protein
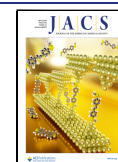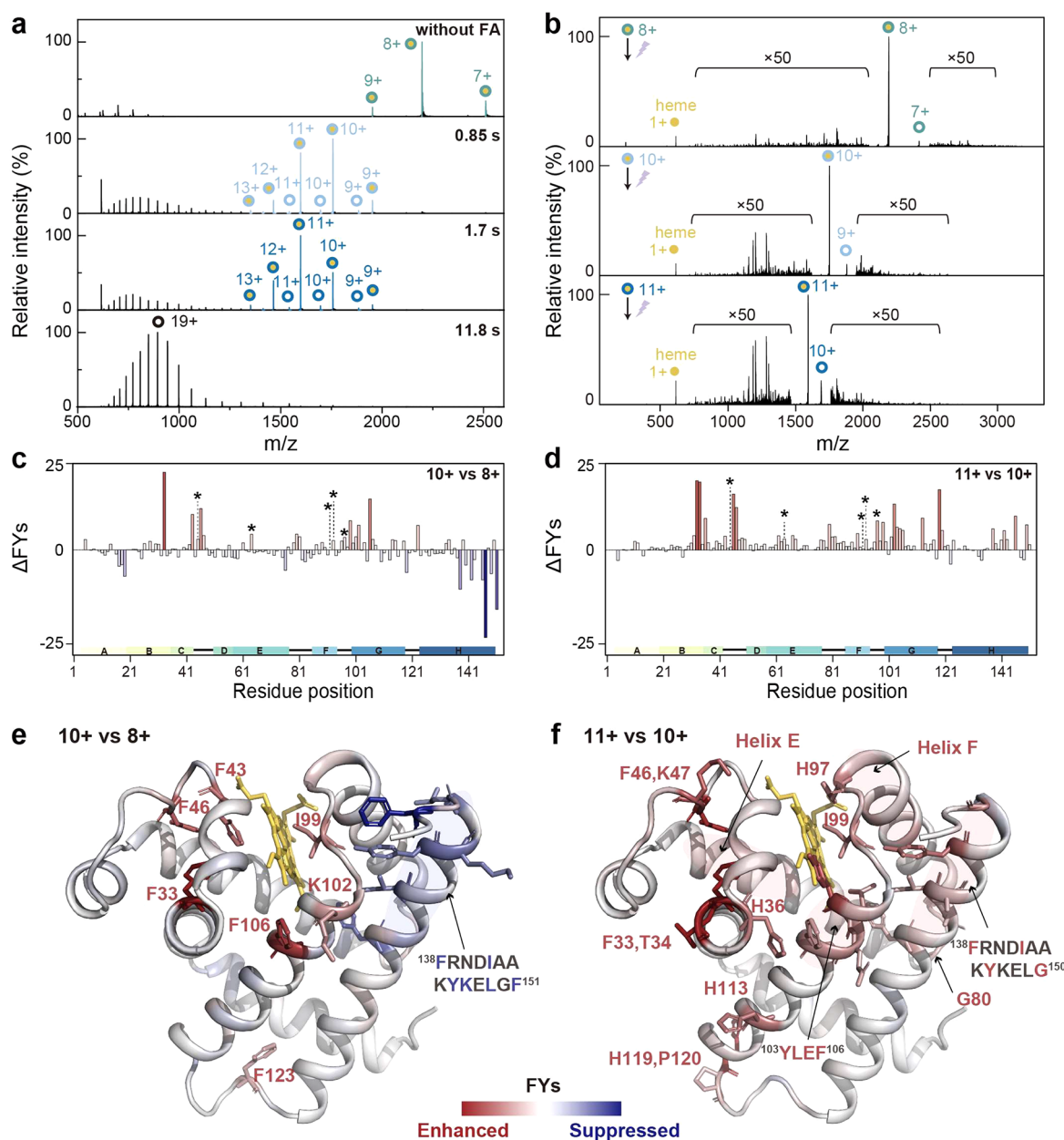
**Figure 2.** (a) TR-nMS characterization of Mb unfolding initiated by online mixing of 20 $\mu$M holo-Mb with 0.02% FA (1:1, v/v) for different mixing times. The filled circle indicates the Mb-heme complex (holo-Mb) while the unfilled circle indicates the Mb without heme (apo-Mb). (b) Representative UVPD spectra of holo-Mb with 8+ (without FA), 10+ (0.85 s), and 11+ (1.7 s) charge states. (c, d) UVPD comparisons of the residue FYs of holo-Mb with 8+, 10+, and 11+ charge states. Residues that are known to interact with heme based on the crystal structure were marked with the symbol "*". Rectangles with different color codes indicate helix A to H. (e, f) Residues with significant FY alterations during the holo-Mb unfolding were mapped on the crystal structure (PDB: 1wla).

structure alterations and protein−protein, protein−ligand interactions.[20−22] On the other hand, collision induced unfolding (CIU) coupled with ion mobility-MS (IM-MS) and variable temperature-ESI MS (VT-ESI MS) are the state-of-art MS strategies for protein stability and structure unfolding analysis with high efficiency.[23−29] Besides, combined with a continuous flow mixing technique, classical subsecond time-resolved ESI-MS can be realized to study the protein folding kinetics.[2,30,31] These MS strategies can characterize the overall changes in protein structures via collision cross sections (CCSs) or charge state distributions (CSDs) but without molecular details.

Dihydrofolate reductase (DHFR) catalyzes the reduction of dihydrofolate (DHF) to tetrahydrofolate (THF) with nicotinamide adenine dinucleotide phosphate (NADPH) as a cofactor.[32] DHFR is involved in purine and thymidylate synthesis and is recognized as an important drug target of diseases such as cancer and rheumatoid arthritis.[33,34] Recently, Cho et al. reported the M42T/H114R mutant (MT-DHFR) was less stable than the wildtype one (WT-DHFR) and was more prone to aggregation through misfolding.[35] However, the molecular mechanisms of M42T/H114R induced stability and structure alterations have not been fully understood.

In this study, we developed a time-resolved nMS (TR-nMS) apparatus by using a capillary-based rapid flow mixer followed
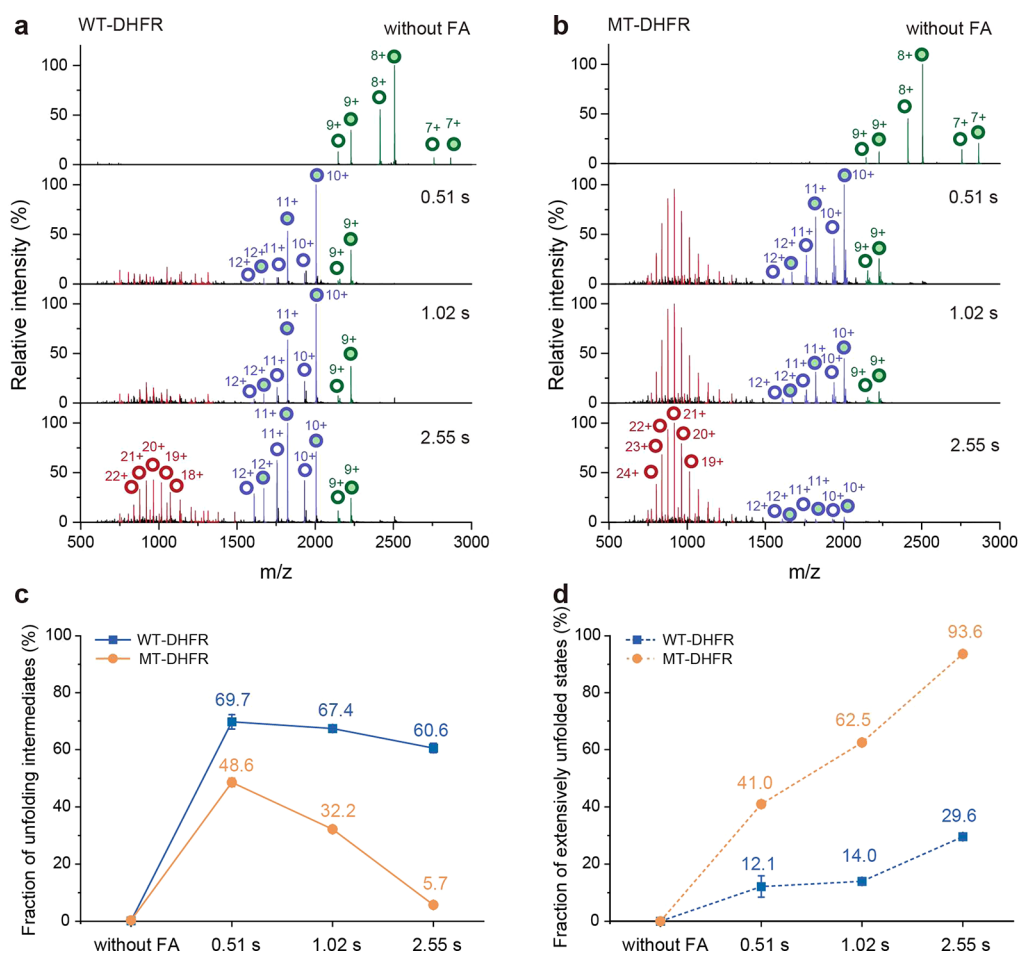
**Figure 3.** TR-nMS characterization of (a) WT- and (b) MT-DHFR unfolding triggered by online mixing of 20 $\mu$M DHFR with 0.1% FA (1:1, v/v) for different mixing times. The filled circle indicates holo-DHFR while the unfilled circle indicates apo-DHFR. Fractions of (c) unfolding intermediates with charge states from 10+ to 12+ and (d) extensively unfolded states with charge states from 13+ to 25+ among the total intensity of all charge states at different mixing times.

with a tip-pulled delay capillary, which could be switched to different lengths and inner diameters to adjust the mixing time of the protein sample with acid solution. The acid-initiated protein unfolding intermediates were transferred into MS by ESI. Then, the specific unfolding intermediate was isolated and subjected to 193 nm UVPD, providing the unfolding molecular details (Figure 1). To test this TR-nMS system, holo-myoglobin (holo-Mb) was introduced, mixed online with 0.02% formic acid (FA) solution for 0.85−11.8 s, and characterized by MS (Figure 2a). Without FA mixing, the CSD of holo-Mb was from 7+ to 9+, with 8+ the most abundant. After mixing with FA solution for 0.85 s, the CSD of holo-Mb unfolding intermediates were mainly shifted to 9+ to 13+, with 10+ the highest form, indicating their compact tertiary structures were mainly retained but with a certain degree of unfolding. Besides, the extensively unfolded apo-Mb ions without heme were also observed in the low mass range with charge states 14+ to 26+. Then, the dominant charge state of unfolding intermediates was shifted to 11+ with 1.7 s FA mixing time. After 11.8 s mixing time, only the denatured apo-Mb ions with 14+ to 26+ charges were observed, indicating their compact structures were totally unfolded. Therefore, this TR-nMS strategy can successfully probe the acid-initiated protein unfolding intermediates with different CSDs at subsecond time scale.

CSDs have been proposed as the representatives of protein structures in solution.[36,37] Thus, the unfolding intermediates [holo-Mb + 10H]$^{10+}$ and [holo-Mb + 11H]$^{11+}$ were subjected to 193 nm UVPD analysis and compared with the original state [holo-Mb + 8H]$^{8+}$ (Figure 2b−f and S1). For [holo-Mb + 10H]$^{10+}$, residues exhibiting the most significant fragmentation yield (FY) alterations were the aromatic residues, which are commonly buried inside the protein hydrophobic core. Briefly, Phe33 in helix B, Phe43 in helix C, Phe46 in C−D loop, Phe106 in helix G, and Phe123 in G−H loop all showed significant FY increases, indicating these regions were prone to unfolding and had extended local structures. Interestingly, several residues around the heme-binding pocket exhibited significant FY decreases including Phe138, Ile142, Tyr146, Lys147, Leu149, and Phe151, demonstrating their local structures became more compact. Thus, it seems there also exists structure refolding around the heme-binding pocket during the initiation of holo-Mb unfolding. Compared with [holo-Mb + 8H]$^{8+}$, strong heme binding could be still retained in [holo-Mb + 10H]$^{10+}$ and the released heme ions in UVPD exhibited little change (Figure 2b). For [holo-Mb + 11H]$^{11+}$, nearly all residues showed significant FY increases and the key regions of heme binding were also unfolded including helix E and F. This was further validated by the weakening of heme binding strength as the ejected heme ions were greatly
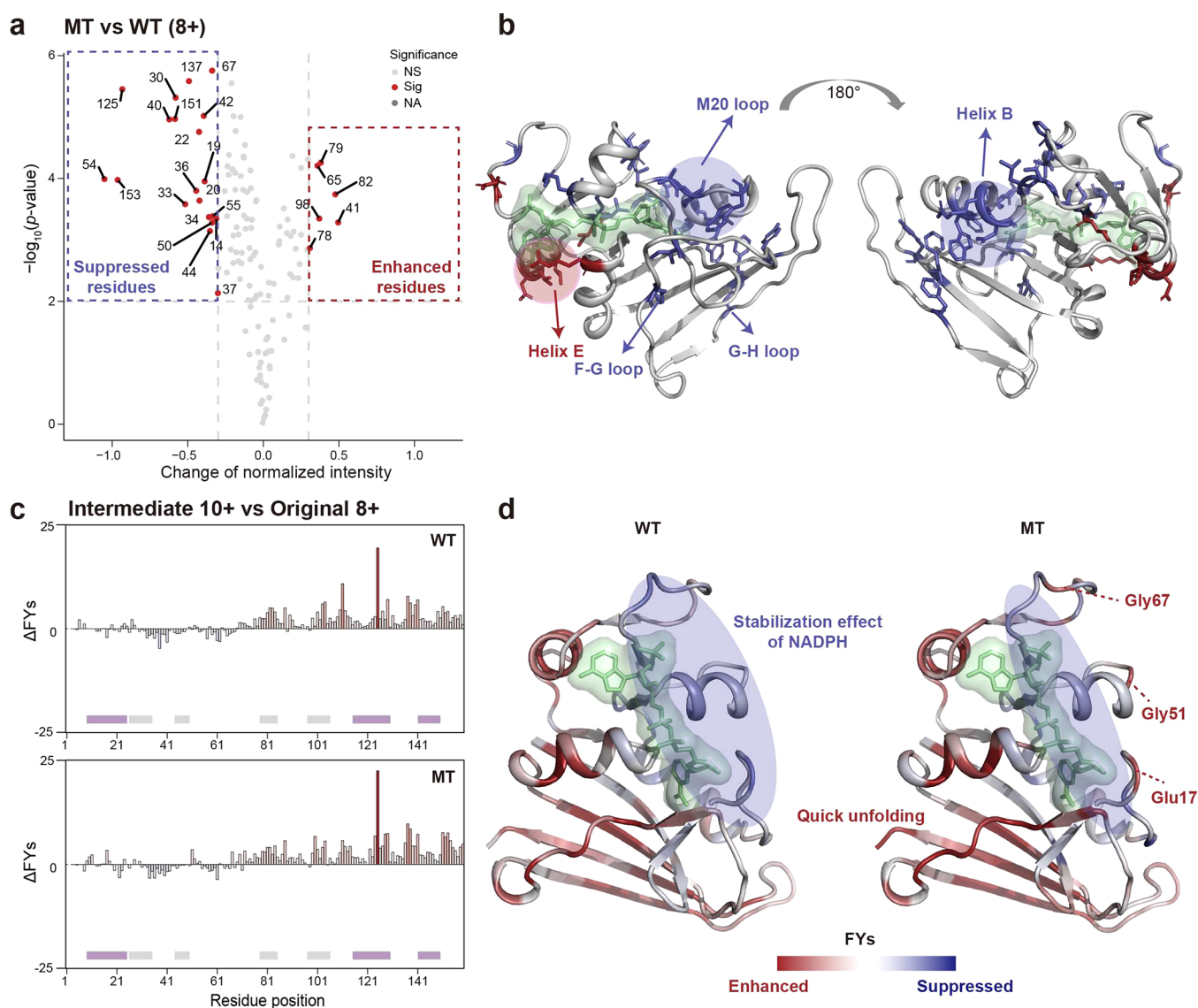
**Figure 4.** (a) Residues with significant fragmentation differences between [holo-DHFR$^{MT}$ + 8H]$^{8+}$ with [holo-DHFR$^{WT}$ + 8H]$^{8+}$ based on the abundances of $a/x$ ions and (b) the results were mapped on the crystal structure of holo-DHFR (PDB: 1rx1). NS, Sig, and NA represent not significant, significant, and not available residues, respectively. (c) UVPD fragmentation propensity comparisons of unfolding intermediate 10+ versus original 8+ of WT- and MT-DHFR based on the summed abundances of $a/x$ ions, and (d) the results were mapped to the crystal structure. Blue indicates suppression, and red indicates enhancement of UVPD FYs. Gray and purple rectangles indicate the well-defined helix and loop regions, respectively.

increased in UVPD (Figure 2b). Therefore, the overall structure of holo-Mb might be unfolded during the second stage of unfolding. The above UVPD results of different unfolding stages are consistent with the sequential mechanism of protein unfolding proposed by Hermans and co-workers.[38−41] Overall, UVPD analysis can provide molecular details in the protein unfolding process.

Next, we applied the TR-nMS system to interrogate the M42T/H114R mutation-induced alterations on the DHFR stability and unfolding dynamics. After online mixing with 0.1% FA solution for 0.51−2.55 s, the gradual unfolding of compact tertiary structures of WT- and MT-DHFR was depicted by the CSDs in MS spectra (Figure 3a, b). Without FA mixing, similar distributions of apo-DHFR and the DHFR-NADPH complex (holo-DHFR) were observed in both WT- and MT-ones with CSDs from 7+ to 9+. It is difficult to differentiate WT- and MT-DHFR stability directly by nMS at

their original states. After mixing with FA solution for 0.51 s, the CSDs of both WT- and MT-DHFR unfolding intermediates were mainly shifted to 10+ to 12+, with 10+ being the highest form. However, extensively unfolded and denatured forms with CSD from 13+ to 25+ were observed only in MT-DHFR, indicating that its stability was much lower than the WT one. When the acid mixing time was increased from 0.51 to 2.55 s, the intensity of unfolding intermediates (CSD 10+ to 12+) was gradually decreased while the intensity of extensive unfolded states (CSD 13+ to 25+) was greatly increased (Figure 3c, d). The WT-DHFR exhibited significantly higher stability in all time points. Particularly, 60.6% unfolding intermediates of WT-DHFR could still be retained, and 29.6% was extensively unfolded even at 2.55 s. In contrast, only 5.7% unfolding intermediates could be retained and 93.6% of the M42T/H114R mutant was serious denatured at 2.55 s (Figure 3c, d). Obviously, our TR-nMS system can

quantitatively characterize the mutation induced stability alterations of the target proteins.

Then, $[holo\text{-}DHFR^{WT} + 8H]^{8+}$ and $[holo\text{-}DHFR^{MT} + 8H]^{8+}$ at their original states without acid mixing were subjected to 193 nm UVPD analysis, which resulted in similar fragmentation patterns and >93% cleavage site coverages (Figure S2), demonstrating the overall structure of holo-DHFR was not significantly affected by the M42T/H114R mutations. We compared the FYs of $a/x$ ions between $[holo\text{-}DHFR^{WT} + 8H]^{8+}$ and $[holo\text{-}DHFR^{MT} + 8H]^{8+}$ (Figure 4a, b). The residues including Ile41, Gln65, Val78, Asp79, Ile82, and Arg98 exhibited significant FY increases, all located around the adenosine group of NADPH. The increased flexibility around NADPH indicates the decrease of ligand-binding strength after the mutations (Figure 4b). On the other hand, the residues with decreased FYs mainly located around the central $\beta$-sheet including Trp30, Arg33, and Asn34 in helix B, Tyr151 in strand H, Phe125 in F—G loop, and Phe137 in G—H loop, implying the increased hydrophobic interactions among these closely distributed secondary structures in holo-DHFR$^{MT}$. The M20 loop also exhibited a flexibility decrease with a higher interaction with the nicotinamide-ribose moiety of NADPH after mutation, indicated by the deceased FYs of Ile14, Ala19, Met20, and Trp22. The decreased flexibility of M20 loop, F—G loop, and G—H loop may make the central $\beta$-sheet more open, resulting in a higher aggregation tendency of holo-DHFR$^{MT}$ (Figure 4b).

Compared with the original $[holo\text{-}DHFR^{WT/MT} + 8H]^{8+}$, the unfolding intermediates $[holo\text{-}DHFR^{WT/MT} + 10H]^{10+}$ showed significant FY increase in the overall structure except for the sequence region from Phe31 to Thr68, indicating the intramolecular interactions were extensively disrupted during the acid-initiated unfolding (Figure 4c, d, and S2). Interestingly, the residues with decreased FYs were mainly located around NADPH, indicating an unusual stabilization effect of NADPH during the initiation of unfolding (Figure 4d). Besides, this stabilization effect was weakened in the mutant as residues Glu17, Gly51, and Gly67 showed significant FY increases only in holo-DHFR$^{MT}$. Thus, the binding strength of NADPH is a key determinant of the unfolding rate. The binding pocket of NADPH unfolds slower than the other parts of DHFR. We also performed UVPD comparisons of the original $[apo\text{-}DHFR^{WT} + 8H]^{8+}$ and $[apo\text{-}DHFR^{MT} + 8H]^{8+}$ (Figure S3 and S4). Most residues in the peripheral region of the apo-DHFR$^{MT}$ central $\beta$-sheet exhibited significant FY increases, indicating enhanced flexibility and weakened local interactions. Interestingly, this region bears most of the basic residues (Figure S5), resulting in a high propensity for unfolding during the acid-initiated denaturation. Thus, apo-DHFR$^{MT}$ unfolding is faster than the WT one. Overall, the lower interactions between NADPH and holo-DHFR$^{MT}$ accelerate the NADPH loss and structure unfolding during acid denaturation compared to the WT one. After NADPH loss, the apo-DHFR$^{MT}$ has weaker intramolecular interactions in the basic region, resulting in a much faster unfolding rate to form the extensively unfolded structures.

In conclusion, we developed a TR-nMS strategy coupled with 193 nm UVPD analysis to interrogate the mutation-induced subtle alterations in protein stability and structure unfolding dynamics. The species and relative intensities of acid-initiated protein unfolding intermediates can be monitored in TR-nMS via their unique CSDs at subsecond time scale. Then, UVPD analysis can interrogate the specific sites and regions involved in the structure unfolding process. We quantitatively evaluated the effects of M42T/H114R mutations on DHFR stability, which could not be directly measured by nMS. In addition, we observed that the cofactor NADPH had an unusual stabilization effect on the DHFR structure during the acid-initiated unfolding process. The M42T/H114R mutations led to a significant decrease in NADPH-DHFR interactions, promoting the structure unfolding rate due to the weaker intramolecular interactions of apo-DHFR$^{MT}$. Our results underscore the great potential of TR-nMS and UVPD analysis in addressing mutation-induced pathological mechanisms and rational drug design.

## ■ ASSOCIATED CONTENT

### Ⓢ Supporting Information

The Supporting Information is available free of charge at https://pubs.acs.org/doi/10.1021/jacs.4c00316.

> Fragmentation patterns and sequence coverages of Mb and DHFR ions, UVPD analysis of $[DHFR^{WT} + 8H]^{8+}$ and $[DHFR^{MT} + 8H]^{8+}$, and basic residues in the apo-DHFR (PDF)

## ■ AUTHOR INFORMATION

### Corresponding Author

**Fangjun Wang** − *CAS Key Laboratory of Separation Sciences for Analytical Chemistry, Dalian Institute of Chemical Physics, Chinese Academy of Sciences, Dalian 116023, China; State Key Laboratory of Molecular Reaction Dynamics, Dalian Institute of Chemical Physics, Chinese Academy of Sciences, Dalian 116023, China; University of Chinese Academy of Sciences, Beijing 100049, China;* ⓘ orcid.org/0000-0002-8118-7019; Email: wangfj@dicp.ac.cn

### Authors

**Pan Luo** − *Institute of Advanced Science Facilities, Shenzhen 518107, China; CAS Key Laboratory of Separation Sciences for Analytical Chemistry, Dalian Institute of Chemical Physics, Chinese Academy of Sciences, Dalian 116023, China; State Key Laboratory of Molecular Reaction Dynamics, Dalian Institute of Chemical Physics, Chinese Academy of Sciences, Dalian 116023, China; Department of Chemical Physics, University of Science and Technology of China, Hefei 230026, China*

**Zheyi Liu** − *CAS Key Laboratory of Separation Sciences for Analytical Chemistry, Dalian Institute of Chemical Physics, Chinese Academy of Sciences, Dalian 116023, China; University of Chinese Academy of Sciences, Beijing 100049, China*

**Can Lai** − *CAS Key Laboratory of Separation Sciences for Analytical Chemistry, Dalian Institute of Chemical Physics, Chinese Academy of Sciences, Dalian 116023, China; State Key Laboratory of Molecular Reaction Dynamics, Dalian Institute of Chemical Physics, Chinese Academy of Sciences, Dalian 116023, China; University of Chinese Academy of Sciences, Beijing 100049, China*

**Zhixiong Jin** − *CAS Key Laboratory of Separation Sciences for Analytical Chemistry, Dalian Institute of Chemical Physics, Chinese Academy of Sciences, Dalian 116023, China; State Key Laboratory of Molecular Reaction Dynamics, Dalian Institute of Chemical Physics, Chinese Academy of Sciences, Dalian 116023, China*

**Mengdie Wang** − *CAS Key Laboratory of Separation Sciences for Analytical Chemistry, Dalian Institute of Chemical Physics, Chinese Academy of Sciences, Dalian 116023, China; University of Chinese Academy of Sciences, Beijing 100049, China*

**Heng Zhao** − *CAS Key Laboratory of Separation Sciences for Analytical Chemistry, Dalian Institute of Chemical Physics, Chinese Academy of Sciences, Dalian 116023, China; State Key Laboratory of Molecular Reaction Dynamics, Dalian Institute of Chemical Physics, Chinese Academy of Sciences, Dalian 116023, China*

**Yu Liu** − *CAS Key Laboratory of Separation Sciences for Analytical Chemistry, Dalian Institute of Chemical Physics, Chinese Academy of Sciences, Dalian 116023, China;* ⊙ orcid.org/0000-0002-0779-1488

**Weiqing Zhang** − *State Key Laboratory of Molecular Reaction Dynamics, Dalian Institute of Chemical Physics, Chinese Academy of Sciences, Dalian 116023, China;* ⊙ orcid.org/0000-0001-6518-4152

**Xingan Wang** − *Department of Chemical Physics, University of Science and Technology of China, Hefei 230026, China;* ⊙ orcid.org/0000-0002-1206-7021

**Chunlei Xiao** − *State Key Laboratory of Molecular Reaction Dynamics, Dalian Institute of Chemical Physics, Chinese Academy of Sciences, Dalian 116023, China;* ⊙ orcid.org/0000-0002-1549-5945

**Xueming Yang** − *Institute of Advanced Science Facilities, Shenzhen 518107, China; State Key Laboratory of Molecular Reaction Dynamics, Dalian Institute of Chemical Physics, Chinese Academy of Sciences, Dalian 116023, China;* ⊙ orcid.org/0000-0001-6684-9187

Complete contact information is available at:
https://pubs.acs.org/10.1021/jacs.4c00316

**Author Contributions**

[#]Pan Luo and Zheyi Liu contributed equally.

**Notes**

The authors declare no competing financial interest.

## REFERENCES

(1) Henzler-Wildman, K.; Kern, D. Dynamic personalities of proteins. *Nature* **2007**, *450* (7172), 964−972.

(2) Lento, C.; Wilson, D. J. Subsecond time-resolved mass spectrometry in dynamic structural biology. *Chem. Rev.* **2022**, *122* (8), 7624−7646.

(3) Hallacli, E.; Kayatekin, C.; Nazeen, S.; Wang, X. H.; Sheinkopf, Z.; Sathyakumar, S.; Sarkar, S.; Jiang, X.; Dong, X.; Di Maio, R.; Wang, W.; Keeney, M. T.; Felsky, D.; Sandoe, J.; Vahdatshoar, A.; Udeshi, N. D.; Mani, D. R.; Carr, S. A.; Lindquist, S.; De Jager, P. L.; Bartel, D. P.; Myers, C. L.; Greenamyre, J. T.; Feany, M. B.; Sunyaev, S. R.; Chung, C. Y.; Khurana, V. The Parkinson's disease protein alpha-synuclein is a modulator of processing bodies and mRNA stability. *Cell* **2022**, *185* (12), 2035−2056.

(4) Zhou, X.; Sumrow, L.; Tashiro, K.; Sutherland, L.; Liu, D.; Qin, T.; Kato, M.; Liszczak, G.; McKnight, S. L. Mutations linked to neurological disease enhance self-association of low-complexity protein sequences. *Science* **2022**, *377* (6601), No. eabn5582.

(5) Li, Y.; Porta-Pardo, E.; Tokheim, C.; Bailey, M. H.; Yaron, T. M.; Stathias, V.; Geffen, Y.; Imbach, K. J.; Cao, S.; Anand, S.; Akiyama, Y.; Liu, W.; Wyczalkowski, M. A.; Song, Y.; Storrs, E. P.; Wendl, M. C.; Zhang, W.; Sibai, M.; Ruiz-Serra, V.; Liang, W.-W.; Terekhanova, N. V.; Rodrigues, F. M.; Clauser, K. R.; Heiman, D. I.; Zhang, Q.; Aguet, F.; Calinawan, A. P.; Dhanasekaran, S. M.; Birger, C.; Satpathy, S.; Zhou, D. C.; Wang, L.-B.; Baral, J.; Johnson, J. L.; Huntsman, E. M.; Pugliese, P.; Colaprico, A.; Iavarone, A.; Chheda, M. G.; Ricketts, C. J.; Fenyo, D.; Payne, S. H.; Rodriguez, H.; Robles, A. I.; Gillette, M. A.; Kumar-Sinha, C.; Lazar, A. J.; Cantley, L. C.; Getz, G.; Ding, L.; Clinical Proteomic Tumor, A. Pan-cancer proteogenomics connects oncogenic drivers to functional states. *Cell* **2023**, *186* (18), 3921−3944.

(6) Hao, G.-F.; Yang, G.-F.; Zhan, C.-G. Structure-based methods for predicting target mutation-induced drug resistance and rational drug design to overcome the problem. *Drug Discovery Today* **2012**, *17* (19−20), 1121−1126.

(7) Vasan, N.; Baselga, J.; Hyman, D. M. A view on drug resistance in cancer. *Nature* **2019**, *575* (7782), 299−309.

(8) Hollingsworth, S. A.; Dror, R. O. Molecular dynamics simulation for all. *Neuron* **2018**, *99* (6), 1129−1143.

(9) Rodrigues, C. H. M.; Pires, D. E. V.; Ascher, D. B. DynaMut: predicting the impact of mutations on protein conformation, flexibility and stability. *Nucleic Acids Res.* **2018**, *46* (W1), W350−W355.

(10) Tamara, S.; den Boer, M. A.; Heck, A. J. R. High-resolution native mass spectrometry. *Chem. Rev.* **2022**, *122* (8), 7269−7326.

(11) Yen, H.-Y.; Liko, I.; Song, W.; Kapoor, P.; Almeida, F.; Toporowska, J.; Gherbi, K.; Hopper, J. T. S.; Charlton, S. J.; Politis, A.; Sansom, M. S. P.; Jazayeri, A.; Robinson, C. V. Mass spectrometry captures biased signalling and allosteric modulation of a G-protein-coupled receptor. *Nat. Chem.* **2022**, *14* (12), 1375−1382.

(12) Oluwole, A. O.; Corey, R. A.; Brown, C. M.; Hernandez-Rocamora, V. M.; Stansfeld, P. J.; Vollmer, W.; Bolla, J. R.; Robinson, C. V. Peptidoglycan biosynthesis is driven by lipid transfer along enzyme-substrate affinity gradients. *Nat. Commun.* **2022**, DOI: 10.1038/s41467-022-29836-x.

(13) Chen, S.; Getter, T.; Salom, D.; Wu, D.; Quetschlich, D.; Chorev, D. S.; Palczewski, K.; Robinson, C. V. Capturing a rhodopsin receptor signalling cascade across a native membrane. *Nature* **2022**, *604* (7905), 384−390.

(14) Bai, Y.; Liu, Z.; Li, Y.; Zhao, H.; Lai, C.; Zhao, S.; Chen, K.; Luo, C.; Yang, X.; Wang, F. Structural Mass Spectrometry Probes the Inhibitor-Induced Allosteric Activation of CDK12/CDK13-Cyclin K Dissociation. *J. Am. Chem. Soc.* **2023**, *145* (21), 11477−11481.

(15) Zhou, L.; Liu, Z.; Guo, Y.; Liu, S.; Zhao, H.; Zhao, S.; Xiao, C.; Feng, S.; Yang, X.; Wang, F. Ultraviolet Photodissociation Reveals the Molecular Mechanism of Crown Ether Microsolvation Effect on the Gas-Phase Native-like Protein Structure. *J. Am. Chem. Soc.* **2023**, *145* (2), 1285−1291.

(16) Chen, X.; Ji, S.; Liu, Z.; Yuan, X.; Xu, C.; Qi, R.; He, A.; Zhao, H.; Song, H.; Xiao, C.; Gao, W.; Chen, P. R.; Luo, R.; Li, P.; Wang, F.; Yang, X.; Tian, R. Motif-dependent immune co-receptor interactome profiling by photoaffinity chemical proteomics. *Cell Chem. Biol.* **2022**, *29* (6), 1024−1036.

(17) Pan, J.; Han, J.; Borchers, C. H.; Konermann, L. Characterizing short-lived protein folding intermediates by top-down hydrogen exchange mass spectrometry. *Anal. Chem.* **2010**, *82* (20), 8591−8597.

(18) Cain, R. L.; Webb, I. K. Online protein unfolding characterized by ion mobility electron capture dissociation mass spectrometry: cytochrome C from neutral and acidic solutions. *Anal. Bioanal. Chem.* **2023**, *415* (5), 749−758.

(19) Wollenberg, D. T. W.; Pengelley, S.; Mouritsen, J. C.; Suckau, D.; Jorgensen, C. I.; Jorgensen, T. J. D. Avoiding H/D scrambling with minimal Ion transmission loss for HDX-MS/MS-ETD analysis

on a high-resolution Q-TOF mass spectrometer. *Anal. Chem.* **2020**, *92* (11), 7453−7461.

(20) Cammarata, M. B.; Thyer, R.; Rosenberg, J.; Ellington, A.; Brodbelt, J. S. Structural Characterization of Dihydrofolate Reductase Complexes by Top-Down Ultraviolet Photodissociation Mass Spectrometry. *J. Am. Chem. Soc.* **2015**, *137* (28), 9128−9135.

(21) Cammarata, M.; Thyer, R.; Lombardo, M.; Anderson, A.; Wright, D.; Ellington, A.; Brodbelt, J. S. Characterization of trimethoprim resistant E-coli dihydrofolate reductase mutants by mass spectrometry and inhibition by propargyl-linked antifolates. *Chem. Sci.* **2017**, *8* (5), 4062−4072.

(22) Brodbelt, J. S.; Morrison, L. J.; Santos, I. Ultraviolet photodissociation mass spectrometry for analysis of biological molecules. *Chem. Rev.* **2020**, *120* (7), 3328−3380.

(23) Zhong, Y.; Han, L.; Ruotolo, B. T. Collisional and Coulombic Unfolding of Gas-Phase Proteins: High Correlation to Their Domain Structures in Solution. *Angew. Chem., Int. Ed.* **2014**, *53* (35), 9209−9212.

(24) Dixit, S. M.; Polasky, D. A.; Ruotolo, B. T. Collision induced unfolding of isolated proteins in the gas phase: past, present, and future. *Curr. Opin. Chem. Biol.* **2018**, *42*, 93−100.

(25) Gadkari, V. V.; Ramirez, C. R.; Vallejo, D. D.; Kurulugama, R. T.; Fjeldsted, J. C.; Ruotolo, B. T. Enhanced collision induced unfolding and electron capture dissociation of native-like protein ions. *Anal. Chem.* **2020**, *92* (23), 15489−15496.

(26) Sipe, S. N.; Lancaster, E. B.; Butalewicz, J. P.; Whitman, C. P.; Brodbelt, J. S. Symmetry of 4-oxalocrotonate tautomerase trimers influences unfolding and fragmentation in the gas phase. *J. Am. Chem. Soc.* **2022**, *144* (27), 12299−12309.

(27) Raab, S. A.; El-Baba, T. J.; Woodall, D. W.; Liu, W.; Liu, Y.; Baird, Z.; Hales, D. A.; Laganowsky, A.; Russell, D. H.; Clemmer, D. E. Evidence for many unique solution structures for chymotrypsin iinhibitor 2: a thermodynamic perspective derived from VT-ESI-IMS-MS measurements. *J. Am. Chem. Soc.* **2020**, *142* (41), 17372−17383.

(28) Walker, T. E.; Shirzadeh, M.; Sun, H. M.; McCabe, J. W.; Roth, A.; Moghadamchargari, Z.; Clemmer, D. E.; Laganowsky, A.; Rye, H.; Russell, D. H. Temperature regulates stability, ligand binding (Mg2+ and ATP), and stoichiometry of GroEL-GroES complexes. *J. Am. Chem. Soc.* **2022**, *144* (6), 2667−2678.

(29) Henderson, L. W.; Sharon, E. M.; Gautam, A. K. S.; Anthony, A. J.; Jarrold, M. F.; Russell, D. H.; Matouschek, A.; Clemmer, D. E. Stability of 20S proteasome configurations: preopening the axial gate. *J. Phys. Chem. Lett.* **2023**, *14* (21), 5014−5017.

(30) Konermann, L.; Collings, B. A.; Douglas, D. J. Cytochrome c folding kinetics studied by time-resolved electrospray ionization mass spectrometry. *Biochemistry* **1997**, *36* (18), 5554−5559.

(31) Sogbein, O. O.; Simmons, D. A.; Konermann, L. Effects of pH on the kinetic reaction mechanism of myoglobin unfolding studied by time-resolved electrospray ionization mass spectrometry. *J. Am. Soc. Mass Spectrom.* **2000**, *11* (4), 312−319.

(32) Sawaya, M. R.; Kraut, J. Loop and subdomain movements in the mechanism of Escherichia coli dihydrofolate reductase: Crystallographic evidence. *Biochemistry* **1997**, *36* (3), 586−603.

(33) Jensen, D. E.; Black, A. R.; Swick, A. G.; Azizkhan, J. C. Distinct roles for Sp1 and E2F sites in the growth/cell cycle regulation of the DHFR promoter. *J. Cell. Biochem.* **1997**, *67* (1), 24−31.

(34) Huennekens, F. M. The methotrexate story—a paradigm for development of cancer chemotherapeutic-agents. In *Advances in Enzyme Regulation*; Weber, G., Ed.; Pergamon Press, 1994; Vol. *34*, pp 397−419.

(35) Cho, Y.; Zhang, X.; Pobre, K. F. R.; Liu, Y.; Powers, D. L.; Kelly, J. W.; Gierasch, L. M.; Powers, E. T. Individual and collective contributions of chaperoning and degradation to protein homeostasis in E. coli. *Cell Rep.* **2015**, *11* (2), 321−333.

(36) Konermann, L.; Rosell, F. I.; Mauk, A. G.; Douglas, D. J. Acid-induced denaturation of myoglobin studied by time-resolved electrospray ionization mass spectrometry. *Biochemistry* **1997**, *36* (21), 6448−6454.

(37) Konermann, L.; Douglas, D. J. Acid-induced unfolding of cytochrome c at different methanol concentrations: Electrospray ionization mass spectrometry specifically monitors changes in the tertiary structure. *Biochemistry* **1997**, *36* (40), 12296−12302.

(38) Shen, L. L.; Hermans, J. Kinetics of conformation change of sperm-whale myoglobin.1. folding and unfolding of metmyoglobin following pH jump. *Biochemistry* **1972**, *11* (10), 1836−1841.

(39) Shen, L. L.; Hermans, J. Kinetics of conformation change of sperm-whale myoglobin. 2. Characterization of rapidly and slowly formed denatured species. *Biochemistry* **1972**, *11* (10), 1842−1844.

(40) Shen, L. L.; Hermans, J. Kinetics of conformation change of sperm-whale myoglobin. 3. folding and unfolding of apomyoglobin and suggested overall mechanism. *Biochemistry* **1972**, *11* (10), 1845−1849.

(41) Konermann, L.; Douglas, D. J. Unfolding of proteins monitored by electrospray ionization mass spectrometry: A comparison of positive and negative ion modes. *J. Am. Soc. Mass Spectrom.* **1998**, *9* (12), 1248−1254.